Journal of Materials Chemistry C

Accepted Manuscript

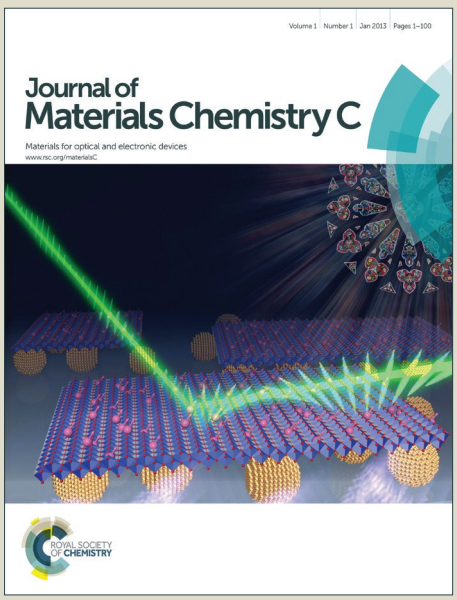

ROYAL SOCIETY OF CHEMISTRY

www.rsc.org/materialsC

Colloidal Synthesis of $Cu_{2-x}Ag_xCdSnSe_4$ Nanocrystals: Microstructures Facilitate High Performance Thermoelectricity

Qiufan Chen,[1] Guiwen Wang,[1] Aijuan Zhang,[1] Dingfeng Yang,[2] Wei Yao,[1] Kunling Peng,[1,2]

Yanci Yan,[1] Xiaonan Sun,[1] Anping Liu[1], Guoyu Wang[2*], Xiaoyuan Zhou[1*]

[1]Department of Applied Physics, Chongqing University, Chongqing 400044, P. R. China.

[2]Chongqing Institute of Green and Intelligent Technology, Chinese Academy of Sciences Chongqing, 400714, P. R. China.

*Corresponding author: Tel: +86-23-6593-5603; Fax: +86-23-6567-8362

Email: xiaoyuan2013@cqu.edu.cn; guoyuw@cigit.ac.cn

Abstract

In this study, we report the colloidal synthesis (CS) of quaternary chalcogenide $Cu_{2-x}Ag_xCdSnSe_4$ nanocrystals (x=0, 0.1, 0.2, 0.3, and 0.4) and their application in thermoelectrics. The as-prepared $Cu_{2-x}Ag_xCdSnSe_4$ nanocrystals present a narrow size distribution ranging from 30 to 50 nm and a precisely controlled composition. Additionally, it was observed that the disordered zinc blende phases were embedded in the normal zinc blende phases and amorphous nanoparticles were dispersed on grain surfaces and between grain boundaries of spark plasma sintered bulk $Cu_{2-x}Ag_xCdSnSe_4$. Moreover, a large enhancement in the Seebeck coefficient and a dramatically reduced lattice thermal conductivity was found in $Cu_{2-x}Ag_xCdSnSe_4$ solid solution, resulting in the dimensionless thermoelectric figure of merit reaching a peak

value of 0.8 at 688 K when x = 0.3. This represents a 44% and 83% improvement in comparison to the un-doped sample and the sample made *via* solid state method (SS), respectively. The results demonstrate an exciting scientific opportunity to raise the figure-of-merit of quaternary chalcogenide $Cu_2CdSnSe_4$ prepared by colloidal synthesis via optimized solid solution.

Key words: Quaternary chalcogenide; Colloidal synthesis; Thermoelectric properties; Nanocrystals.

1. Introduction

The confluence of energy demands and environmental preservation has spurred research into renewable technologies that will allow for an eventual transition away from fossil fuels as the primary source of energy. One such avenue lies in the area of thermoelectric (TE) materials, which can convert waste industrial heat into electricity.[1-3] The efficiency of TE materials is determined by the dimensionless figure-of-merit $ZT=S^2\sigma T/\kappa$, where S is the Seebeck coefficient, σ the electrical conductivity, and κ the thermal conductivity. To achieve high ZT requires a material with a high power factor $PF = S^2\sigma$ and a very low thermal conductivity.[4] The problem is that the transport parameters are interdependent and, often, attempts to maximize one parameter have a deleterious effect on the other parameters.

Recently, a class of quaternary chalcogenide compounds I_2-II-IV-VI_4 (I=Ag, Cu; II=Zn, Cd; IV=Si, Ge, Sn; VI=S, Se, Te) with the diamond-like structure and a wide band gap has been found to have reasonable thermoelectric performance as *p*-type thermoelectric materials.[5-10] Similar to ternary Cu_2MSe_3, the structure of this

compound can also be derived from the cubic zinc blende binary II-VI compounds through substituting atoms of group II by atoms of both group I and group III, followed by a further substitution two group III atoms with one atom of group II and one atom of group IV.[11] Figure 1 shows the crystal structure of $Cu_2CdSnSe_4$. Zn layers in the ZnS cubic structure are cross-substituted by ordered Cu-Cd/Sn atoms, leading to a stannite phase with the space group $I\bar{4}2m$.

The band gap of quaternary chalcogenides such as $Cu_2CdSnSe_4$ is around 1.0 eV, a relatively large value compared with that of the traditional narrow band gap thermoelectric materials, such as PbTe (0.32 eV) and Bi_2Te_3 (0.16 eV).[12-15] Thus, quaternary chalcogenides demonstrate a relatively low electrical conductivity. However, the lattice thermal conductivity is also low due to strong phonon scattering by the intrinsically complex bonding type and/or the highly distorted crystal structure in these materials, yielding a relatively attractive thermoelectric performance. As such, considerable attention has been drawn to these quaternary compounds. So far, the best *ZT* value of 0.91 at 700 K was achieved with Cu-rich $Cu_{2.1}Zn_{0.9}SnSe_4$,[16] very close to the figure of merit of *p*-type thermoelectric materials such as skutterudites and commercial Bi_2Te_3.

It is worthwhile to note that the above mentioned quaternary compounds have been, so far, synthesized by the traditional solid state method (SS). This process is time and energy consuming, and typically takes several days to prepare a densified product. Besides, the grain size attained by the SS is typically on the scale of several micrometers. It is well known that reducing the grain size is, indeed, a powerful way to greatly suppress the lattice thermal conductivity and thus improve the overall thermoelectric performance. In contrast, the colloidal synthesis (CS) has been widely used to successfully prepare chalcogenide nanocrystals.[17] Thereby, CS of $Cu_2CdSnSe_4$

nanocrystals and their subsequent compaction into dense samples could be considered an effective way to enhance their thermoelectric performance due to a significant reduction in the thermal conductivity associated with the increased grain boundary density. This, of course, assumes that the phonon mean-free path is reduced to a greater extent than the mean-free path of electrons. Another advantages related to the CS of $Cu_2CdSnSe_4$ nanocrystals as far as thermoelectric applications are concerned are: (1) the potential decoupling of the Seebeck coefficient from the electrical conductivity; (2) an enhancement in the Seebeck coefficient as a result of energy-dependent scattering of electrons at the interface of nanocrystals; (3) solution based processing methods that are, indeed, helpful in reducing the cost and allowing for the manipulation of grains size and shape. In this scenario, CS is particularly advantageous for the fabrication of quaternary chalcogenide thermoelectrics, and comparable in their influence to inorganic solar absorbers in photovoltaics and photodetector devices.[18-26] Currently, the vast majority of such studies have focused on the effect of doping and vacancy on Cd, Sn or Se sites, aiming to optimize the thermoelectric properties. A peak ZT value of 0.65 at 723 K in $Cu_{2.1}Cd_{0.8}SnSe_{3.4}$[27] and 0.71 at 685 K in $Cu_{2.15}Cd_{0.85}SnSe_{3.9}$[28] have been obtained. Apart from that, to the best of our knowledge, reports on the CS of chalcogenide nanocrystals for thermoelectric application are rare.

In this work, we report on the significantly improved thermoelectric performance of quaternary chalcogenide compounds $Cu_{2-x}Ag_xCdSnSe_4$ with x=0, 0.1, 0.2, 0.3, and 0.4 via the wet-chemistry synthesis method followed by spark plasma sintering. The improvement is accomplished because (a) the thermal conductivity is greatly reduced by stronger phonon scattering resulting from the increased grain boundary density achieved by the solution-based synthesis of nanocrystals and the presence of

amorphous nanoparticles dispersed on the grains and between grain boundaries; (b) the Seebeck coefficient is enhanced due to the energy filtering effect whereby the low energy electrons are scattered by the interface formed between the disordered zinc blend phase and the cubic zinc blende phase in $Cu_{2-x}Ag_xCdSnSe_4$ solid solution. These two factors boost the *ZT* of $Cu_{2-x}Ag_xCdSnSe_4$ up to 0.8 at 688 K when $x = 0.3$. Herein, it is believed that the Ag atoms substitute on sites of Cu and maintain the minimum distortion of the lattice and its overall energy stability.

2. Experimental Section

2.1 Chemicals

Copper acetylacetonate (reagent grade, 97%), cadmium acetate dihydrate (reagent grade, 99.99%), silver acetate (99.95%), selenium dioxide (99%), oleylamine (80%-90%) were purchased from Aladdin, acetylacetone tin (IV) dichloride salt (reagent grade, 98%), 1-octadecene (tech, 90%) were provided by Tansoole. All chemicals were stored in the glove box and used as received without further purification.

2.2 Synthesis

Cations which included copper acetylacetonate (3.9-2*x* mmol, *x*=0, 0.1, 0.2, 0.3, and 0.4), silver acetate (*x* mmol), cadmium acetate dihydrate (1 mmol), acetylacetone tin (IV) dichloride salt (1.8 mmol) were dissolved in 10 mL oleylamine under vacuum condition. This solution was heated to 413 K and maintained at this temperature for 30 minutes under vacuum. Afterward, the temperature of this mixture was dropped to 373 K and kept at this temperature until selenium solution was injected. The anion was obtained by dissolving selenium dioxide in 1-octadecene under vacuum at 353 K

until the color of this solution became orange. Then, the temperature of the selenium solution was reduced to around 330 K and rapidly injected into the reaction flask, which contained the cation solution. Following the injection, the temperature was raised to 583 K under the flow of nitrogen maintained at this temperature for 30 minutes. Finally, the solution was cooled naturally to 330 K, where the color of the mixture changed from deep blue to yellow-brown and eventually to the black color, indicating the formation of the $Cu_{2-x}Ag_xCdSnSe_4$ nanocrystals. The resulting solution was isolated by centrifugation at 8000 rpm for 5 minutes to obtain pure $Cu_{2-x}Ag_xCdSnSe_4$ samples. Before centrifugation, the obtained black precipitate was dispersed in hexane 20 mL and sonicated at 300 K for 15 minutes. This process was repeated five times until the prepared nanocrystals' precipitate could no longer be dispersed in hexane. In order to thoroughly remove the surfactant, the product was then washed by 20 mL hydrazine monohydrate and 20 mL hexane followed by centrifugation. This process was repeated three times. Finally, the washed samples were dried out in the vacuum dryer with the typical yield of about 0.8 g per run. More than 3 g of as-prepared $Cu_{2-x}Ag_xCdSnSe_4$ nanocrystals were densified by spark plasma sintering (SPS) with a graphite die (Φ=10 mm) at 730 K for 5 minutes under a pressure of 45 MPa. The density of the obtained bulk sample is up to 5.1 g/cm.

2.3 Structure and thermoelectric characterization

Thermal diffusivity (λ) was obtained by the laser flash method (Netzsch LFA-457), and converted into thermal conductivity (κ) using $\kappa = \lambda C_p d$, where C_p is the specific heat measured in a differential scanning calorimeter, Netzsch, 404 F3. A value of 0.31

J/g/K is used in this study. The sample density *d* was determined using the Archimedes method. High temperature electrical conductivity (σ) and the Seebeck coefficient (*S*) were measured on rectangular-shaped samples in the interval 300 K to 750 K using a commercial system (LSR-3, Linseis). Powder X-ray diffraction patterns were collected using PANalytical X'pert apparatus with Co Ka radiation. The morphology and microstructure were investigated using Field Emission Scanning Electron Microscopy (JSM-7800F, JEOL) and transmission electron microscopy (JEM2100F).

3. Results and Discussion

3.1 Structure characterization.

Shown in Figure 2 (a) are the X-ray diffraction patterns of as-prepared $Cu_{2-x}Ag_xCdSnSe_4$(x=0, 0.1, 0.2, 0.3, and 0.4) powders. All diffraction peaks can be indexed to those of PDF#52-869, indicating the formation of crystalline single phase $Cu_2CdSnSe_4$ structure without the presence of any impurity phases. According to the XRD spectra and using the Scherrer equation, the size of these nanocrystals is estimated as 30 nm in diameter for all five samples. Nitro sorption isotherms revealed that samples possessed specific surface area of approximately ~10 m^2/g. Figures 2(b) and 2(c) show the typical scanning electron microscopy (SEM) and transmission electron microscopy (TEM) images of the colloidal synthesized nanocrystals. The as-prepared nanocrystals are narrowly distributed and the average size of the nanoparticles is in the range of 30-50 nm. It should be noted that (1) the excellent size control of the particle sizes achieved by this wet chemistry approach gives us the

opportunity to better explore the influence of the isoelectronic substitution of Ag for Cu on the thermoelectric performance of $Cu_{2-x}Ag_xCdSnSe_4$ solid solutions; (2) the specific size of as-prepared nanoparticles is dependent on both the species and the concentration of precursor solutions as well as the temperature and the volume of the reaction vessel adopted for the nanocrystals growth. The processing conditions with respect to the temperature and the soaking time are of prime concern and determine the quality of the final product. High resolution transmission electron microscopy (HRTEM) and selected area electron diffraction (SAED) patterns are shown in Figure 2(d) and indicate that the as-prepared nanocrystals are mainly of zinc-blende (ZB) structure.

Figure 3 shows the phase and morphology of the SPS sintered $Cu_{2-x}Ag_xCdSnSe_4$ compounds. Judging from Figure 3 (a), no new crystal phase nor any phase segregation was noticed after sintering. Namely, these patterns are indexed to the $Cu_2CdSnSe_4$ structure with the space group $I\bar{4}2m$ and a= 5.832 Å in the tetragonal system. Furthermore, the lattice expansion is expected upon Ag replacing Cu atoms. However, as shown in Figure 3(a), no peak shift was observed with the increasing level of Ag concentration, indicating the lattice parameters remained identical for all $Cu_{2-x}Ag_xCdSnSe_4$ compounds. This, in turn, indicates the disappearance of the built-up lattice strain which might otherwise have a detrimental effect on the electronic mobility.[29, 30]

Figure 3 (b) shows the typical fracture surface morphology of $Cu_{2-x}Ag_xCdSnSe_4$ samples compacted by SPS. It is evident that our samples possess densely packed

grains with the size around 50 - 100 nm and only very few pores. Nitro sorption isotherms indicated that samples possessed specific surface area of approximately~18 m^2/g. It is worth noting that the grain size of our $Cu_{2-x}Ag_xCdSnSe_4$ is more uniform and much reduced in comparison to the grain size of samples made by SS. Such a difference is anticipated based on the fact that our as-prepared powder for SPS is made by CS which exhibits narrowly distributed grain sizes from 30 to 50 nm. Such reduction in the grain size is supposed to be extremely helpful in lowering the lattice thermal conductivity. Evidently, some regrowth of nanoparticles is observed after the heat treatment during SPS. Figure 3(c) and 3(d) are the low magnification TEM images of $Cu_{2-x}Ag_xCdSnSe_4$ samples for x = 0 and 0.3, respectively. It is noted that these two samples possess clear grain boundaries. However, in the $Cu_{2-x}Ag_xCdSnSe_4$ solid solution, a few amorphous nanoparticles with the diameter of around 10-20 nm are shown on the surface of grains and between grain boundaries, a feature completely absent in the sample with no Ag element. Scanning TEM (STEM) in combination with energy dispersive X-ray spectroscopy (EDS) can be used to compare each element concentration in the amorphous nanoparticles with that in the matrix, although the situation is somewhat complicated by not being able to determine exactly the composition of individual amorphous nanoparticles because of their overlap with the matrix. The EDX results indicate the composition of the amorphous nanoparticles, which exhibit that these small particles are Ag rich and Cd/Sn poor as compared to those conventional nano-counterparts. The non-stoichiometric element compositions, which intrinsically exhibit the spatial charge inhomogeneity, lead to the formation of

those amorphous particles. Figure 3(e) displays high-resolution TEM images of the $Cu_{1.7}Ag_{0.3}CdSnSe_4$ sample. The inset in Figure 3(e) shows the corresponding selective area diffraction (SAD) pattern. As demonstrated in Figure 3(e), the lattice spacing in the (*112*) plane is the same as in the as-prepared powders, indicating that the majority zinc blende structure is maintained in bulk $Cu_{1.7}Ag_{0.3}CdSnSe_4$. However, the disordered zinc blende phase is nevertheless present as circled in Figure 3(e). Energy dispersive X-ray (EDX) was also conducted on the $Cu_{1.7}Ag_{0.3}CdSnSe_4$ sample. As indicated in Figure 3(f), Ag is clearly present in our $Cu_{1.7}Ag_{0.3}CdSnSe_4$ compounds. Additionally, the composition of this grain is consistent with the data obtained by ICP characterization shown in Table 1.

3.2 Electric transport properties

Temperature dependence of the electrical conductivity (σ) and the Seebeck coefficient (S) for $Cu_{2-x}Ag_xCdSnSe_4$ compounds with x = 0, 0.1, 0.2, 0.3, and 0.4 are plotted in Figure 4. As comparison, the electrical conductivity (σ), and the Seebeck coefficient (S) for the $Cu_2CdSnSe_4$ compound synthesized via SS is also present in Figure 4. Figure 4(a) shows that all samples have a positive Seebeck coefficient, indicating that the majority carriers are holes. It can also be seen that the Seebeck coefficient of samples made by CS is significantly lower than that of the sample prepared by SS. This trend is consistent with reports in the literature.[16, 27] Moreover, the Seebeck coefficient of $Cu_{2-x}Ag_xCdSnSe_4$ solid solutions increases with the increasing temperature except for sample with x = 0.3, which has a peak value at 662 K. Meanwhile, the Seebeck coefficient of $Cu_{2-x}Ag_xCdSnSe_4$ compounds increases

with the increasing amount of Ag content till *x* reaches up to 0.3. Further increasing Ag content reduces the Seebeck coefficient. In contrast to the Seebeck coefficient of 172 μV/K at 742 K for the sample of *x*=0, the Seebeck coefficients of 133, 194, 262 and 245 μV/K were obtained for samples with *x* of 0.1, 0.2, 0.3 and 0.4, respectively. One factor for the increase of the Seebeck coefficient in $Cu_{2-x}Ag_xCdSnSe_4$ solid solutions is the band engineering effect associated with the presence of disordered zinc blende structure. As depicted in Figure 3(e), the disordered zinc blende phase is embedded in the zinc blende phase. As such, band bending at the disordered zinc blende (DZB) /zinc blende (ZB) interface might produce a scattering potential that could preferentially scatter low energy charge carriers, leading to the enhancement of the Seebeck coefficient, just as was the case with Pb nanoparticles in PbTe.[31] The influence of DZB/ZB blende interface on the propagation of charge carrier is schematically illustrated in Figure 4(c).

Electrical conductivity of $Cu_{2-x}Ag_xCdSnSe_4$ compounds with *x*=0, 0.1, 0.2, 0.3, and 0.4 is shown in Figure 4(b). It is found that (1) the electrical conductivity of the sample made by SS is substantially lower than that of samples made by CS. (2) Apart from the sample with $x = 0.1$, the $Cu_{2-x}Ag_xCdSnSe_4$ solid solution reduces the electrical conductivity. More specifically, the electrical conductivity initially increases from ~16790 S/m to ~28108 S/m at 740 K for samples with $x = 0$ and 0.1, respectively. Subsequently, it decreases to 11694 S/m, 5700 S/m and 6922 S/m for $Cu_{2-x}Ag_xCdSnSe_4$ compounds with *x* equal to 0.2, 0.3 and 0.4, respectively. By introducing the Ag atom into the compound, it is actually a kind of optimizing

strategy in the aspect of the valence band maximum (VBM). In our compounds (I_2CdSnSe$_4$ (I=Cu and Ag)), the VBM is dominated by the strong *p*-*d* hybridization between Cu/Ag *d* and Se *p* orbitals, which forms conductive network for carrier transport. *d* electrons in the Ag-participated compounds are much delocalized than those in Cu-dominated materials, leading to a relatively weak *p*-*d* hybridization and a rather low electrical conductivity.[32] (3) Instead of the monotonic variation of the electrical conductivity with temperature, $Cu_{2-x}Ag_xCdSnSe_4$ compounds with x = 0, 0.1 and 0.2 exhibit peak values at about 590 K, which perhaps results from a phase transformation of $Cu_{2-x}Ag_xCdSnSe_4$, a similar phenomenon reported in the $Cu_2CdSnSe_4$ system.[27] The highest power factor is obtained for samples when x=0.3, reaching its maximum of 0.65 $mWK^{-2}m^{-1}$ at around 565K.

3.3 Thermal transport properties

Figure 5 (a) shows the temperature dependence of the thermal conductivity κ of $Cu_{2-x}Ag_xCdSnSe_4$ obtained from equation $\kappa = \lambda C_p d$, and the inset in Fig. (a) displays the thermal diffusivity λ. Due to the dominance of Umklapp scattering at high temperatures, the total thermal conductivity decreases with the increasing temperature over the measured range up to 723 K. It is noticed that the total thermal conductivity of $Cu_2CdSnSe_4$ SS compounds is higher than that of CS prepared compounds at temperatures lower than 573 K. As the temperature increases, the total thermal conductivity of both CS samples and SS sample is similar because of the extremely reduced electrical conductivity of the SS sample. In addition, as expected, the total thermal conductivity of each sample made by CS is, indeed, low as shown in Figure

5(a), indicating the complexity of the crystallographic structure of the $Cu_2CdSnSe_4$-based compounds and the large density of grain boundary interfaces, which provides extra phonon scattering centers and significantly reduces thermal conductivity. Furthermore, except for $Cu_{1.9}Ag_{0.1}CdSnSe_4$, which has a relatively high thermal conductivity due to a much higher electrical conductivity, the thermal conductivity of solid solutions at their working temperature around 723 K is remarkably decreased, reaching a minimum of 0.37 $Wm^{-1}K^{-1}$ for the $Cu_{1.7}Ag_{0.3}CdSnSe_4$ compound, a reduction by ~38% compared with the sample of x=0. The total thermal conductivity, $\kappa = \kappa_e + \kappa_l$, can be divided into two major components: the electronic component κ_e is due to the heat transported by electrons and the lattice component κ_l is due to the heat transported by phonons. The electronic thermal conductivity was estimated using the Wiedemann-Franz law $\kappa_e = L\sigma T$, where σ is electrical conductivity, L is the Lorenz number, and T is the absolute temperature. The Lorenz number, which depends on the degree of elasticity in carrier scattering, can be calculated from[33]

$$L = \left(\frac{k_B}{e}\right)^2 \left[\frac{\left(r+\frac{7}{2}\right)F_{r+\frac{5}{2}}(\xi)}{\left(r+\frac{3}{2}\right)F_{r+\frac{1}{2}}(\xi)} - \left(\frac{\left(r+\frac{5}{2}\right)F_{r+\frac{3}{2}}(\xi)}{\left(r+\frac{3}{2}\right)F_{r+\frac{1}{2}}(\xi)} \right)^2 \right] \quad (1)$$

where r is the scattering factor which gives the exponent of the energy dependence on the charge carrier mean free path, with a value of -1/2 for the acoustic phonon scattering in the $Cu_2CdSnSe_4$system. $F_n(\xi)$ is the Fermi integral defined as,

$$F_n(\xi) = \int_0^\infty \frac{x^n}{1+e^{x-\xi}} dx \quad (2)$$

where ξ is the reduced Fermi energy that can be deduced from the Seebeck

coefficients and the scattering factor based on the following formula,

$$S = \pm \frac{\kappa_B}{e}\left[\frac{\left(r+\frac{5}{2}\right)F_{r+\frac{3}{2}}(\xi)}{\left(r+\frac{3}{2}\right)F_{r+\frac{1}{2}}(\xi)} - \xi\right] \quad (3)$$

Here it is assumed that the $Cu_2CdSnSe_4$ system can be treated using a single parabolic band model.

The calculated Lorenz number as function of temperature is plotted in the top right inset of Figure 5(b). The lattice thermal conductivity, calculated by subtracting the electronic part from the total thermal conductivity is shown in Figure 5(b). It is noted that κ_e takes a very small fraction of the total thermal conductivity owing to the relatively low electrical conductivity in $Cu_{2-x}Ag_xCdSnSe_4$ compounds. As shown in Figure 5(b), the lattice thermal conductivity of samples prepared by CS is much lower than the conductivity of the sample synthesized by SS in the whole temperature range measured. Such trend is reasonable due to the grain size of the CS sample is dramatically smaller than that of the SS sample. Moreover, with Ag substitution, one achieves a dramatic reduction in the lattice thermal conductivity in comparison to the un-doped sample. In comparison to samples of x = 0, the value of κ_l is reduced by 36%, 22%, 15% and -18% at 723 K, respectively. This reduction is due to: (1) Ag substitution on sites of Cu that introduces point defects which, in turn, enhances phonon scattering (Rayleigh-type scattering) [34]; (2) Ag substitution on Cu sites further distorts the crystallographic structure, which raises its degree of disorder, resulting in stronger scattering of phonons; (3) Nanostructured disordered zinc blende phases embedded in the tetragonal zinc blende phases and Ag-rich nanoparticles on the

surface of grains and between grain boundaries all provide extra phonon scattering centers for mid-to-long wavelength phonons and thus further reduce the thermal conductivity.

The dimensionless thermoelectric figure of merit *ZT* of our samples is calculated based on the above transport data and is plotted in Figure 6. It is found that the *ZT* values increase with the increasing temperature in the measured temperature range. Among samples with the different amount of Ag substitutions, the sample with $x = 0.3$ reaches the highest *ZT* of around 0.8 at ~688 K, the value higher than previously reported magnitudes of *ZT*.[7, 8] Specifically, this is approximately 44%, 53%, 5% and 35% enhancement in *ZT* compared to the figure of merit of samples with $x = 0$, 0.1, 0.2, and 0.4, respectively. The improvement in the figure of merit is attributed to: (a) Solution-processed $Cu_{2-x}Ag_xCdSnSe_4$ nanocrystals densified by SPS which leads to the formation of the reduced grain size ranging from 50 to 100 nm which, in turn, provides extra phonon scattering centers and lowers the lattice thermal conductivity. Besides, Ag-rich nanoparticles with the size from 10-30 nm further enhance phonon scattering, resulting in the much reduced lattice thermal conductivity; (b) the energy filtering effect caused by the interface between the disordered zinc blende phase and the normal zinc blende phases upon Ag substitution enhances the Seebeck coefficient. This simultaneous enhancement in the Seebeck coefficient and the diminished ability of phonons to conduct heat results in an improved thermoelectric figure of merit of $Cu_{2-x}Ag_xCdSnSe_4$ compounds, in spite of the reduced electrical conductivity in these samples. As such, further improvements in *ZT* of $Cu_2CdSnSe_4$ based materials could

be obtained by (1) optimizing both the wet-chemistry and the SPS process to obtain much sharper and cleaner grains and grain boundaries in the final densified bulk product, thereby promoting facile charge transport; (2) varying substitution elements and their amount to simultaneously improve the charge carrier mobility and the carrier density and/or to seek potential resonance states in $Cu_2CdSnSe_4$-based materials to greatly enhance the Seebeck coefficient; (3) further decreasing the thermal conductivity by forming bulk nanocomposites, where various forms of nanoinclusions are uniformly dispersed in the $Cu_2CdSnSe_4$ matrix to scatter phonons over a much broader range of frequencies.

Conclusions

$Cu_{2-x}Ag_xCdSnSe_4$ nanocrystals have been successfully synthesized via the colloidal synthesis method. The as-prepared nanocrystals have a nearly uniform particle size with diameters ranging from 30-50 nm. Some regrowth of $Cu_{2-x}Ag_xCdSnSe_4$ nanoparticles occurs after spark plasma sintering, leading to a particle size of 50-100 nm. It is found that the optimized Ag substitution could enhance the Seebeck coefficient and reduce the thermal conductivity simultaneously, yielding a higher *ZT* of up to 0.8 at 688 K when $x = 0.3$. Further enhancements of thermoelectric properties are possible by optimizing our wet chemistry procedure and substitution in $Cu_2CdSnSe_4$-based compounds.

Acknowledgements

The work was financially supported in part by the National Natural Science

Foundation of China (Grant no. 11344010, 11404044, 51472036, 51401202), and the Fundamental Research Funds for the Central Universities (CQDXWL-2013-Z010). This work at the Chongqing Institute of Green and Intelligent Technology, Chinese Academy of Sciences is supported by the One Hundred Person Project of the Chinese Academy of Science, Grant No. 2013- 46.

References

1. J.-S. Rhyee, K. H. Lee, S. M. Lee, E. Cho, S. I. Kim, E. Lee, Y. S. Kwon, J. H. Shim and G. Kotliar, *Nature*, 2009, **459**, 965-968.
2. G. J. Snyder and E. S. Toberer, *Nat. Mater.*, 2008, **7**, 105-114.
3. R. Venkatasubramanian, E. Siivola, T. Colpitts and B. O'Quinn, *Nature*, 2001, **413**, 597-602.
4. G. J. Snyder and T. S. Ursell, *Phys. Rev. Lett.*, 2003, **91**, 148301.
5. F. S. Liu, J. X. Zheng, M. J. Huang, L. P. He, W. Q. Ao, F. Pan and J. Q. Li, *Sci. Rep.*, 2014, **4**, 5774.
6. F. S. Liu, B. Wang, W. Q. Ao, Y. Li and J. Q. Li, *Intermetallics*, 2014, **55**, 15-21.
7. R. R. Zamani, M. Ibánez, M. Luysberg, N. García-Castelló, L. Houben, J. D. Prades, V. Grillo, R. E. Dunin-Borkowski, J. R. Morante and A. Cabot, *ACS nano*, 2014, **8**, 2290-2301.
8. L. Wu, F.-J. Fan, M. Gong, J. Ge and S.-H. Yu, *Nanoscale*, 2014, **6**, 3418-3422.
9. S. Chen, A. Walsh, Y. Luo, J.-H. Yang, X. Gong and S.-H. Wei, *Phys. Rev. B*, 2010, **82**, 195203.
10. T. Ito, *Jpn. J. Appl. Phys.*, 1998, **37**, L1217-L1220.
11. F.-J. Fan, L. Wu and S.-H. Yu, *Energy Environ. Sci.*, 2014, **7**, 190-208.
12. C. Sevik and T. Çağın, *Appl. Phys. Lett.*, 2009, **95**, 2105.
13. T. C. Harman, B. Paris, S. E. Miller and H. L. Goering, *J. Phys. Chem. Solids*, 1957, **2**, 181-190.
14. S. Yuan, H. Krenn, G. Springholz and G. Bauer, *Phys. Rev. B*, 1993, **47**, 7213-7226.
15. S. Ahn, S. Jung, J. Gwak, A. Cho, K. Shin, K. Yoon, D. Park, H. Cheong and J. H. Yun, *Appl. Phys. Lett.*, 2010, **97**, 021905.
16. M.-L. Liu, I.-W. Chen, F.-Q. Huang and L.-D. Chen, *Adv. Mater.*, 2009, **21**, 3808-3812.
17. F.-J. Fan, Y.-X. Wang, X.-J. Liu, L. Wu and S.-H. Yu, *Adv. Mater.*, 2012, **24**, 6158-6163.
18. D. Aldakov, A. Lefrançois and P. Reiss, *J. Mater. Chem. C*, 2013, **1**, 3756-3776.
19. Y. Liu, J. Xu, Z. Ni, G. Fang and W. Tao, *J. Alloy. Compd.*, 2015, **630**, 23-28.
20. S. E. Habas, H. A. Platt, M. F. van Hest and D. S. Ginley, *Chem. Rev.*, 2010, **110**, 6571-6594.
21. I. Gur, N. A. Fromer, M. L. Geier and A. P. Alivisatos, *Science*, 2005, **310**, 462-465.
22. P. Jackson, D. Hariskos, E. Lotter, S. Paetel, R. Wuerz, R. Menner, W. Wischmann and M. Powalla, *Prog. Photovoltaics*, 2011, **19**, 894-897.
23. Q. Guo, G. M. Ford, R. Agrawal and H. W. Hillhouse, *Prog. Photovoltaics*, 2013, **21**, 64-71.
24. C. Steinhagen, M. G. Panthani, V. Akhavan, B. Goodfellow, B. Koo and B. A. Korgel, *J. Am. Chem. Soc.*, 2009, **131**, 12554-12555.

25. H. Katagiri, K. Jimbo, S. Yamada, T. Kamimura, W. S. Maw, T. Fukano, T. Ito and T. Motohiro, *Appl. Phys. Express*, 2008, **1**, 041201.
26. Q. Guo, G. M. Ford, W.-C. Yang, B. C. Walker, E. A. Stach, H. W. Hillhouse and R. Agrawal, *J. Am. Chem. Soc.*, 2010, **132**, 17384-17386.
27. F.-J. Fan, B. Yu, Y.-X. Wang, Y.-L. Zhu, X.-J. Liu, S.-H. Yu and Z. Ren, *J. Am. Chem. Soc.*, 2011, **133**, 15910-15913.
28. M. Ibáñez, D. Cadavid, R. Zamani, N. García-Castelló, V. Izquierdo-Roca, W. Li, A. Fairbrother, J. D. Prades, A. Shavel and J. Arbiol, *Chem. Mater.*, 2012, **24**, 562-570.
29. M. S. Dresselhaus, G. Chen, M. Y. Tang, R. G. Yang, H. Lee, D. Z. Wang, Z. F. Ren, J. P. Fleurial and P. Gogna, *Adv. Mater.*, 2007, **19**, 1043-1053.
30. S. K. Bux, J.-P. Fleurial and R. B. Kaner, *Chem. Commun.*, 2010, **46**, 8311-8324.
31. J. P. Heremans, C. M. Thrush and D. T. Morelli, *Phys. Rev. B*, 2004, **70**, 115334.
32. L. Xi, Y. B. Zhang, X. Y. Shi, J. Yang, X. Shi, L. D. Chen, W. Zhang, J. Yang and D. J. Singh, *Phys. Rev. B*, 2012, **86**, 155201.
33. T. Dahal, Q. Jie, Y. Lan, C. Guo and Z. Ren, *Phys. Chem. Chem. Phys.*, 2014, **16**, 18170-18175.
34. C. T. Walker and R. O. Pohl, *Phys. Rev.*, 1963, **131**, 1433-1442.

Figure and Table Captions

Figure 1. Crystal structure of $Cu_2CdSnSe_4$

Figure 2.(*a*) X-ray diffraction patterns of $Cu_{2-x}Ag_xCdSnSe_4$ (x=0, 0.1, 0.2, 0.3, 0.4) nanoparticles; (*b*) Typical SEM image of as-prepared $Cu_{2-x}Ag_xCdSnSe_4$ nanoparticles; (*c*) Low-magnification image of powders; (*d*) High-magnification image of nanoparticles and selected-area electron diffraction pattern (inset of *d*).

Figure 3. (*a*) X-ray diffraction patterns of bulk $Cu_{2-x}Ag_xCdSnSe_4$ (x=0,0.1,0.2,0.3,0.4); (*b*) SEM image of bulk $Cu_{2-x}Ag_xCdSnSe_4$; (*c*) Low magnification TEM image of the $Cu_2CdSnSe_4$ sample; (*d*) Low magnification TEM image of the $Cu_{1.7}Ag_{0.3}CdSnSe_4$ sample; (*e*) High-magnification image of the bulk $Cu_{1.7}Ag_{0.3}CdSnSe_4$ sample and selected-area electron diffraction pattern (inset of *e*); (*f*) Energy dispersive X-ray (EDX) of the bulk sample with x=0.3.

Figure 4. Temperature dependence of (*a*) Seebeck coefficient; (*b*) Schematic diagram illustrating energy filtering effect introduced by the wurtzite/zinc blende interface; (*c*) electrical conductivity of $Cu_{2-x}Ag_xCdSnSe_4$ with x=0(■) , 0.1(●), 0.2(▲), 0.3(▼), 0.4(◆). The insets in Figures 4 (*a*) and 4 (*b*) compare the SS sample with the CS sample.

Figure 5. Temperature dependence of the total thermal conductivity κ and the lattice thermal conductivity κ_l for $Cu_{2-x}Ag_xCdSnSe_4$ with x=0(■), 0.1(●), 0.2(▲), 0.3(▼), 0.4(◆). The insets in Figures 5 (*a*) and 5 (*b*) provide a comparison between the SS sample and the CS sample, thermal diffusivities and also depict the calculated temperature-dependent Lorenz number L.

Figure 6. Temperature dependence of the figure of merit ZT for $Cu_{2-x}Ag_xCdSnSe4$ with x=0(■), 0.1(●), 0.2(▲), 0.3(▼), 0.4(◆). The inset in Figure 6 compares the ZT of samples SS and CS.

Table 1. Chemical compositions of $Cu_{2-x}Ag_xCdSnSe_4$ obtained by ICP and the calculated chemical formula based on the measurement.

Table 1. Chemical compositions of $Cu_{2-x}Ag_xCdSnSe_4$ obtained by ICP and the calculated chemical formula based on the measurement.

x	Cu (μg/ml)	Ag (μg/ml)	Cd (μg/ml)	Sn (μg/ml)	Se (μg/ml)	Chemical formula
0	7.48	0	2.92	6.11	15.56	$Cu_2Ag_0Cd_{0.44}Sn_{0.86}Se_{3.34}$
0.1	6.08	0.71	2.11	6.33	14.13	$Cu_{1.9}Ag_{0.14}Cd_{0.38}Sn_{1.06}Se_{3.58}$
0.2	5.12	1.12	2.00	5.88	12.71	$Cu_{1.8}Ag_{0.22}Cd_{0.4}Sn_{1.11}Se_{3.58}$
0.3	5.96	2.08	2.06	4.42	15.58	$Cu_{1.7}Ag_{0.35}Cd_{0.33}Sn_{0.67}Se_{3.58}$
0.4	6.96	3.44	2.78	5.68	19.11	$Cu_{1.6}Ag_{0.46}Cd_{0.36}Sn_{0.7}Se_{3.51}$

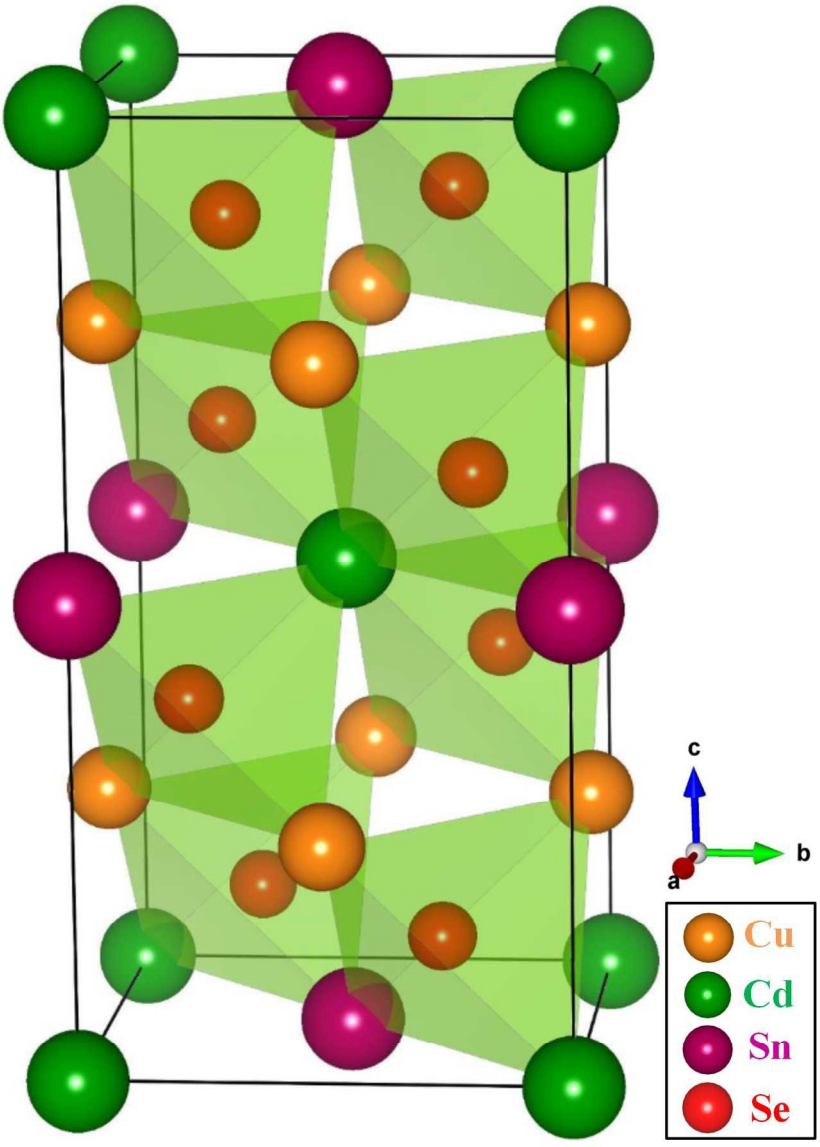

454x629mm (96 x 96 DPI)

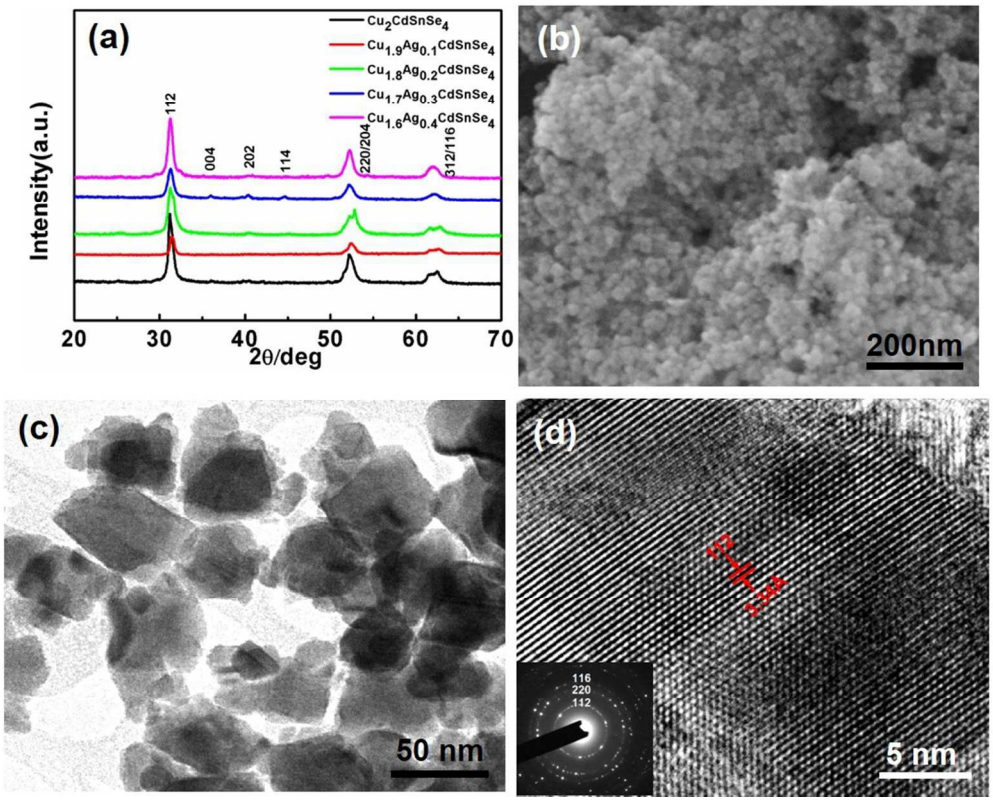

183x145mm (150 x 150 DPI)

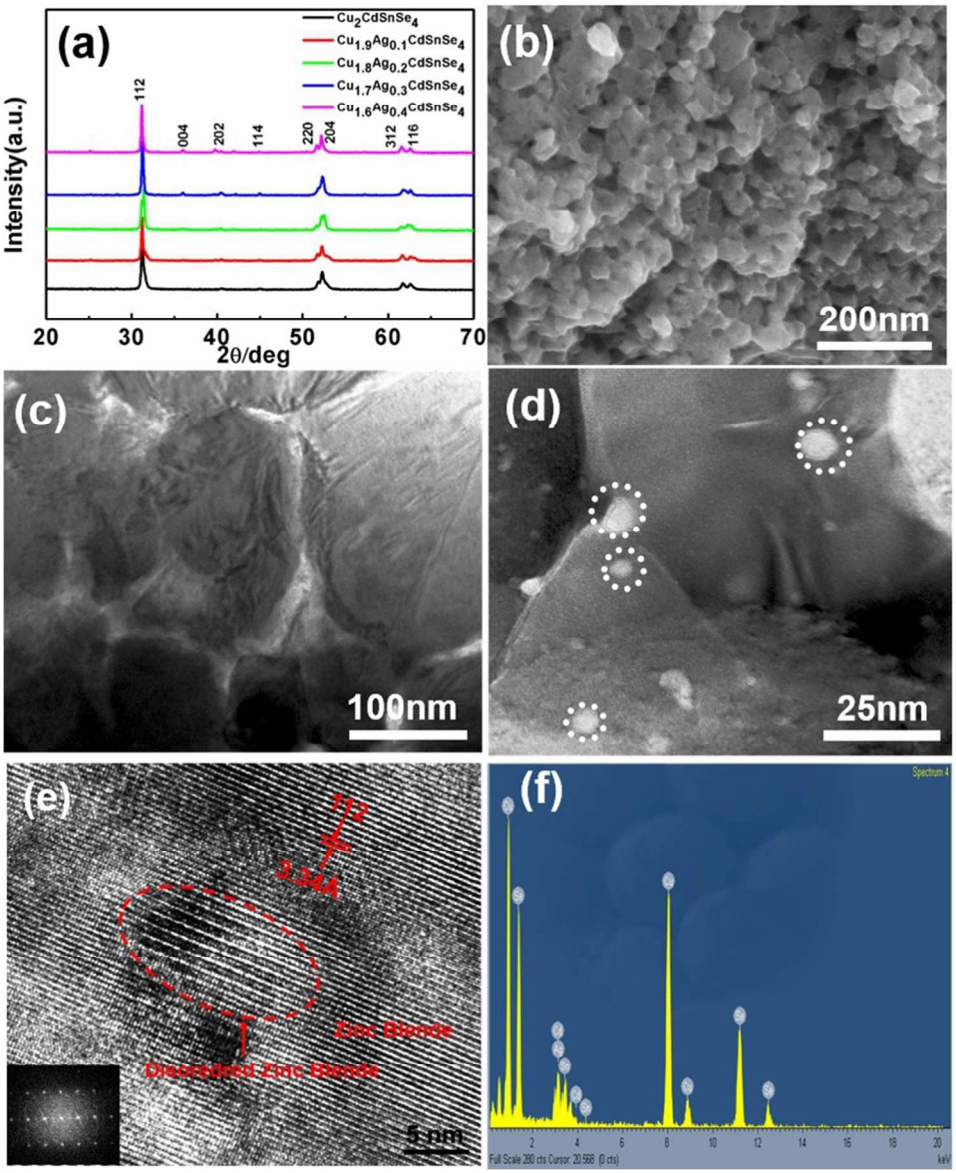

290x340mm (82 x 82 DPI)

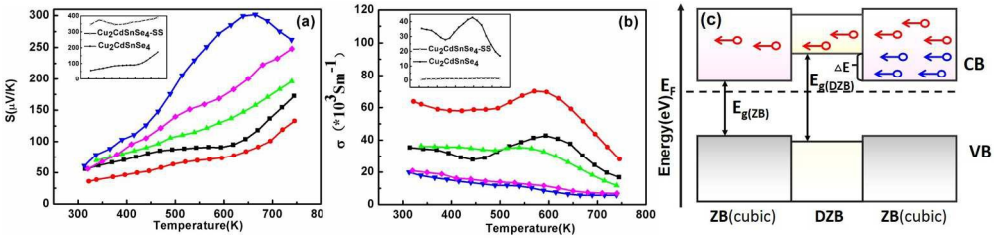

363x87mm (150 x 150 DPI)

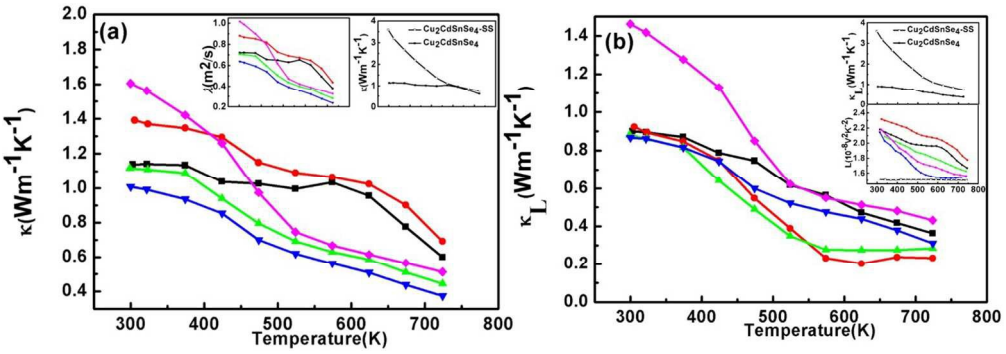

247x85mm (150 x 150 DPI)

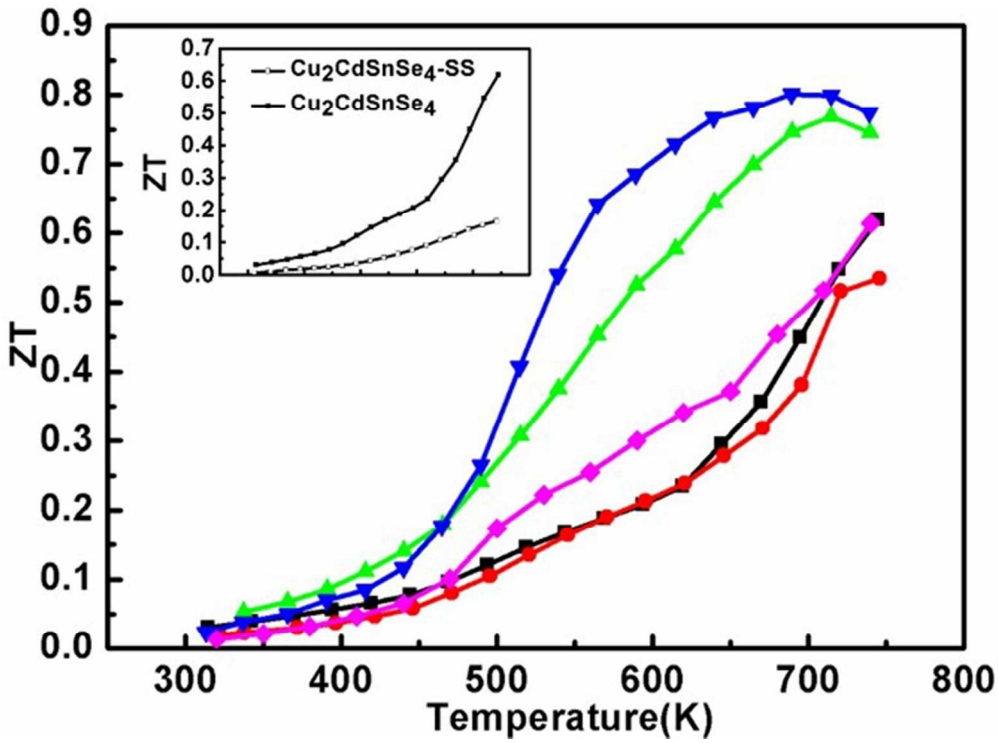

113x83mm (150 x 150 DPI)

In this paper, we have demonstrated how quaternary chalcogenide $Cu_{2-x}Ag_xCdSnSe_4$ nanocrystals can result in spectacular decreases in the lattice thermal conductivity while increasing the Seebeck coefficient. A ZT up to 0.8 was obtained when x is equal 0.3.